PAPER • **OPEN ACCESS**

Facile growth of high-yield and -crystallinity vertically aligned carbon nanotubes via a sublimated ferric chloride catalyst precursor

To cite this article: Hilal Goktas *et al* 2023 *Nano Futures* **7** 025001

View the article online for updates and enhancements.

You may also like

- A novel field emission microscopy method to study field emission characteristics of freestanding carbon nanotube arrays
Yunhan Li, Yonghai Sun, David A Jaffray et al.
- Vertically aligned carbon nanotube arrays as thermal interface material for vibrational structure of piezoelectric transformer
Lie Chen, Bin Ju, Zhihua Feng et al.
- Novel growth method of carbon nanotubes using catalyst-support layer developed by alumina grit blasting
Hiromichi Watanabe, Juntaro Ishii and Keishin Ota

This content was downloaded from IP address 80.251.45.167 on 23/04/2023 at 22:14

NANO FUTURES

PAPER

Facile growth of high-yield and -crystallinity vertically aligned carbon nanotubes via a sublimated ferric chloride catalyst precursor

Hilal Goktas[1,2,3], **Noa Lachman**[4,5,*], **Estelle Kalfon-Cohen**[4], **Xiaoxue Wang**[1,6], **Stephen Torosian**[2], **Karen K Gleason**[1] and **Brian L Wardle**[4,7]

[1] Department of Chemical Engineering, MIT , Cambridge, MA 02139, United States of America
[2] FDA Winchester Engineering and Analytical Center Winchester, 109 Holton St., Winchester, MA 01890, United States of America
[3] Department of Biomedical Engineering, Ankara University, Golbasi, Ankara, Turkey
[4] Department of Aeronautics and Astronautics, MIT, Cambridge, MA 02139, United States of America
[5] Department of Materials Science and Engineering, TAU, Tel-Aviv, 6997801, Israel
[6] Department of Chemical and Biomolecular Engineering, The Ohio State University, Columbus, OH 43210, United States of America
[7] Department of Mechanical Engineering, MIT, Cambridge, MA 02139, United States of America
[*] Author to whom any correspondence should be addressed.

E-mail: noala@tauex.tau.ac.il

Keywords: sublimation of ferric chloride, Carbon nanotubes synthesis, electrical properties, carbon nanotube arrays, vertically-aligned carbon nanotubes

Supplementary material for this article is available online

OPEN ACCESS

RECEIVED
13 January 2023

REVISED
17 February 2023

ACCEPTED FOR PUBLICATION
14 March 2023

PUBLISHED
7 April 2023

Original content from this work may be used under the terms of the Creative Commons Attribution 4.0 licence.

Any further distribution of this work must maintain attribution to the author(s) and the title of the work, journal citation and DOI.

Abstract

A facile and effective catalyst deposition process for carbon nanotube (CNT) array growth via chemical vapor deposition using a resistively heated thermal evaporation technique to sublimate $FeCl_3$ onto the substrate is demonstrated. The catalytic activity of the sublimated $FeCl_3$ catalyst precursor is shown to be comparable to the well-studied e-beam evaporated Fe catalyst, and the resulting vertically aligned CNTs (VA-CNTs) have a similar diameter, walls, and defects, as well as improved bulk electrical conductivity. In contrast to standard e-beam-deposited Fe, which yields base-growth CNTs, scanning and transmission electron microscopy and X-ray photoelectron spectroscopy characterizations reveal a tip-growth mechanism for the $FeCl_3$-derived VA-CNT arrays/forests. The $FeCl_3$-derived forests have a lower (∼1/3 less) longitudinal indentation modulus, but higher longitudinal electrical conductivity (greater than twice) than that of the e-beam Fe-grown CNT arrays. The sublimation process to grow high-quality VA-CNTs is a highly facile and scalable process (extensive substrate shape and size, and moderate vacuum and temperatures) that provides a new route to synthesizing aligned CNT forests for numerous applications.

1. Introduction

Considered one of the best-known mechanical materials, carbon nanotubes (CNTs) possess unique structural and electrical properties that make them ideal for a wide variety of applications, including sensing [1], energy storage [2], and membrane separation [3]. Vertically aligned CNTs (VA-CNTs) are directly grown on a substrate where population dynamics determine the resulting aligned CNT array or forest structure. Horizontally aligned CNTs (HA-CNTs) can also be synthesized directly on a substrate or obtained by post-processing VA-CNTs or floating-catalyst-grown CNTs [4]. This highly organized arrangement is particularly beneficial to applications where anisotropy is required, e.g. for mechanical and electrical applications, where properties along the nanofibers in the array can be very different than perpendicular to the fibers.

Of the various methods available for VA-CNT growth, thermal catalytic chemical vapor deposition (CCVD) is one of the most promising techniques. The CCVD method is widely utilized to study the scaling of nanoscale material properties to the bulk scale [5, 6]. In this process, a deposited catalyst precursor seed is

© 2023 The Author(s). Published by IOP Publishing Ltd

annealed in a reducing atmosphere at 700 °C. Hydrocarbon gas feedstock is then introduced, initiating CNT growth via nucleation of carbon atoms on the reduced catalyst [5]. After a short phase of random growth (also known as 'the crust'), the high density of CNTs restricts the direction of the carbon crystal growth, creating a highly oriented array of CNTs conforming to population dynamics [7, 8]. Commonly used catalyst species are iron (Fe), cobalt (Co), and nickel (Ni). These metals show both a high solubility of carbon and a high rate of carbon diffusion [9]. As a result, and under typical VA-CNT synthesis conditions, metastable metal carbides form, providing the release of carbon atoms [10]. The high catalytic effect of iron on hydrocarbon decomposition provides a higher VA-CNT yield, and thus the use of iron catalysts dominates for both multiwall and single-wall CNTs [11].

Deposition of iron catalysts is still an active research area as it has a direct impact on the structure and therefore properties, working toward practical applications such as organic synthesis, the petrochemical industry, reducing agents in gas and water pollution, power generation, pharmacy, and the development of advanced functional materials [12]. Common procedures involve the deposition of continuous iron films by either physical or chemical methods [13], both yielding efficient growth of well-defined VA-CNT forests along with a controlled CNT diameter and number of layers, and a somewhat controlled chirality. Physical methods include the physical vapor deposition (PVD) of metal such as electron beam (e-beam) evaporation [14] and ion beam sputtering [15]. PVD methods can provide nanoscale control of the catalyst precursor layer (from 1 to 10 nm) while yielding excellent adherence to the substrate [16] but at the cost of an extremely slow deposition rate (around 0.05 nm s^{-1} or less depending on the type of metal). The requirement for a high vacuum (∼1.0 mTorr) is another drawback of PVD.

Alternatively, an organometallic compound such as ferrocene or iron pentacarbonyl can be employed as a catalyst precursor. Catalyst particles 4.0–6.5 nm in dimension form in the gas phase from the thermal decomposition of the organometallic compound at modest pressure (∼7.5 mTorr) [17, 18]. When using a common double-stage furnace, the precursor vaporizes in the first zone and is transported to the second zone where the precursor decomposes and VA-CNTs are synthesized. However, using an organometallic precursor usually results in catalyst deposition throughout the VA-CNT forest, discontinuous CNTs, and if targeting single-walled CNTs [19], no specific chirality. Removal of the catalyst, if necessary, is a complicated procedure.

Chemical VA-CNT synthesis methods include electrodeposition [20], impregnation [21], dip-coating of Fe salt [22] and protein (ferritin) [23], or $FeCl_3$ solution [22, 23] casting. Studies on $FeCl_3$ catalyst precursors showed that poly(dimethyl siloxane) can be used to stamp the precursor from a solution of $FeCl_3$ in ethanol or methanol. Solution-based catalyst precursor deposition requires no complex equipment, but the surface tension effects that are present in the liquid phase can make it difficult to wet low surface energy substrates or even moderately complex topographies [24]. An all-dry chemical method for the synthesis of VA-CNTs utilizes iron chloride ($FeCl_2$) powder placed directly onto the substrate as a catalyst precursor without any additional catalyst process [25, 26]. Inoue *et al* reported that $FeCl_2$ maintained at a vacuum of 1.0 mTorr during annealing at 800 °C starts to vaporize at 550 °C, and is entirely spread into the system at 800 °C [25, 26]. When acetylene is introduced into the system, the reaction of acetylene with vaporized $FeCl_2$ produces Fe_3C and related carbon-rich iron carbide that nucleates into nanoparticles. Those nanocatalysts can be directly deposited onto many substrates for future CNT growth. Inoue *et al* report the successful growth of CNT forests with this method; however, they also report the observation of residual Fe and Fe_3C (impurities) in the CNT forest [25].

Here, we present the synthesis and characterizations of VA-CNTs produced by CCVD using a sublimated ferric chloride ($FeCl_3$) catalyst in an attempt to limit the residual impurities and demonstrate a conformal process for complex topographies. We selected $FeCl_3$ as a catalyst precursor for its lower vapor pressure during its sublimation and dissociation enthalpy compared to $FeCl_2$ [27, 28]. Sublimation of $FeCl_3$ is carried out by a resistively heated crucible at a moderate vacuum (∼0.1 Torr) onto the substrate, which is then immediately introduced to the CCVD reactor. At the CCVD CNT nucleation stage, $FeCl_3$ is expected to decompose into $FeCl_2$ above 500 and reduce to Fe above 600 °C [29]. The moderate vacuum and low substrate temperature of the sublimation process enable conformal deposition of $FeCl_3$ oxidized polymer thin film onto virtually any type of substrate including both planar and nonplanar three-dimensional (3D) surfaces [30]. Utilizing this approach, and the ability to conformally sublimate $FeCl_3$ on 3D surfaces (see growth on woven alumina fabric discussion and figure S1 in supplemental information), we also compared the growth mechanism of VA-CNTs with traditional e-beam evaporated Fe and sublimated $FeCl_3$ under identical CCVD conditions. The adherence force between the catalyst and the substrate is one of the key parameters to determine the structure of the grown VA-CNTs: a base growth of VA-CNTs is promoted by a strong catalyst–substrate adhesion where the catalyst remains anchored to the substrate during the growth, while a tip growth is observed when the catalyst lifts off the substrate and is seen at the top of the VA-CNTs due to weak catalyst–substrate adhesion [15, 31]. Thus, a difference in the adherence forces between e-beam

evaporated Fe and sublimated $FeCl_3$ could result in different growth mechanisms, enabling further tailoring of the final VA-CNT properties.

2. Experimental section

2.1. Catalyst sublimation procedure

$FeCl_3$ was sublimated by a resistively heated crucible on an Al_2O_3 thin film (10 nm) coated silicon wafer attached to a downward-facing stage that was held at a constant temperature of 80 °C and 100 °C at a moderate vacuum (∼0.1 Torr) [32], then immediately introduced to the CCVD reactor.

The new catalyst procedure is compared to our standard e-beam growth [33] on a 10 nm Al_2O_3/1 nm Fe bilayer thin film catalyst deposited by e-beam evaporation on a bare silicon wafer at 1×10^{-7} Torr.

2.2. Growth of VA-CNTs

VA-CNT arrays were grown on 1 cm^2 silicon wafers prepared as described above in a 44 mm diameter quartz tube furnace at atmospheric pressure via thermal catalytic CVD with C_2H_4 gas as a carbon feedstock, and H_2 and He as gas carriers. The wafers were then introduced into the quartz tube and the furnace was heated up to the growth temperature of 740 °C under H_2 and water vapor at flow rates of 1040 sccm and 15 sccm, respectively. When the furnace reached the target temperature, the gas inlet was switched to pure C_2H_4 at a flow rate of 400 sccm for a period in the range of 30 s to 5 min.

2.3. Materials characterization

The catalyst precursor layers were investigated by load sensing nanoindentation (Hysitron, TriboIndenter, USA) using a Berkovitch tip. Both sublimated $FeCl_3$ 100 °C and e-beam deposited Fe were tested. A rule of thumb in nanoindentation implies that the minimum indentation depth should be at least 10% of the thickness of the tested film. To fulfill this requirement, both substrates were coated with 50 nm Al_2O_3 and 200 nm of $FeCl_3$ and Fe, respectively. The experiment was set as follows: first, the area function of the indenter was calibrated on fused quartz. Then the indenter was loaded at a rate of 2 nm s^{-1} into the substrate, held for 10 s at 20 nm indentation depth (to rule out the effect of Al_2O_3 and silicon), and then the indenter was unloaded while simultaneously recording the load. At least 50 indentations were performed on each substrate. When the 50 indentations were completed, a final calibration of the area function of the tip was done on quartz. Hardness was calculated for both substrates as follows:

$$H = \frac{P}{24.5\,h_c^2}. \tag{1}$$

The hardness was systematically computed using equation (1), with P being the maximal load and h_c the contact depth.

Nanoindentation gives hardness and an inferred modulus; thus, in the course of this testing, qualitative observations were made on the relative compliance and strength of the e-beam vs. sublimated $FeCl_3$ films, serving as an indirect assessment of the potential adhesion of the precursors, later confirmed by scanning electron micrograph (SEM) images. SEMs were taken by a field emission gun scanning electron microscope (Zeiss Ultra Plus) under 0.5 kV–1.5 kV. Transmission electron micrographs (TEMs) were taken by an aberration-corrected transmission electron microscope (Libra, Zeiss) operated at 80 kV. Statistical analysis of CNT morphology was conducted using Origin software, based on normal distribution. Raman spectra were taken with a Horiba LabRam HR (Model 800) at a wavelength of 513 nm to characterize the aligned CNTs. I_D/I_G was calculated by integrating the area under the peaks [34].

Angle-resolved X-ray photoelectron spectroscopy (XPS) analysis was performed in a ultra high vacuum (UHV) chamber (PHI Versaprobe II XPS) with a scanning monochromated Al source (117.4 eV, 47.1 W, spot size 200.0 μm). The depth-dependent chemical composition of the samples was determined by sputtering the surface (4 min) using the instrument's $C_{60}+$ ion source (10 kV 20 nA). Peak analysis and quantification were carried out by CasaXPS software.

2.4. Electrical measurements

The sheet resistance of knocked-down VA-CNT forests (HA-CNTs) [4] was measured using four point probes (Keithley) and the average sheet resistance was compiled from at least five samples.

3. Results and discussion

Substrates with Fe deposited by e-beam (e-beam-Fe) were compared to substrates coated with $FeCl_3$ sublimated at a 100 °C (sub-Fe-100) or 80 °C (sub-Fe-80) stage temperature. Microscopic inspection of the

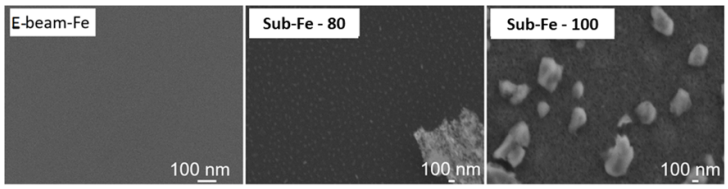


Figure 1. SEMs of the iron catalyst film deposited on silicon wafer by e-beam deposition (e-beam-Fe) or $FeCl_3$ sublimation at 80 °C and 100 °C (sub-Fe-80 and sub-Fe-100, respectively).

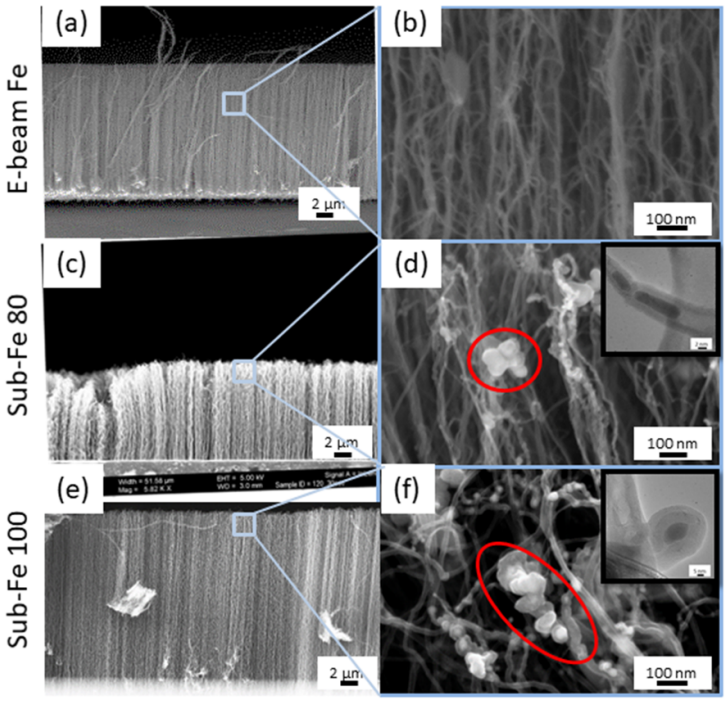


Figure 2. SEM images of CNTs grown on the e-beam-Fe (a) and (b), on sub-Fe-80 (c) and (d), and on sub-Fe-100 (e) and (f). Fe nanoparticles are seen at the top of the sub-Fe-grown CNT forest ((d) and (f), encircled in red), and can also be seen in the TEM inset of the top of the forests. For all three samples, VA-CNT growth was performed at 740 °C for 30 s.

surface displays evidence of large particle clusters when the catalyst precursor was deposited at 100 °C. This is further confirmed in high-resolution SEM images in figure 1, which show the formation of a continuous catalyst precursor layer with larger particles (∼300 nm) spread across the surface. When deposited at 80 °C, no underlying continuous film is observed but, rather, the $FeCl_3$ particles formed seem to be smaller (∼10–30 nm) and uniformly distributed. These continuous films with embedded larger particles in the Fe sublimation compare to the uniform continuous Fe film from e-beam deposition. It is well known that, prior to CNT growth, metal films de-wet in the reducing environment of the growth chamber, forming nanoparticles that are the catalyst seeds for CNT growth, with CNT diameter corresponding approximately to catalyst nanoparticle diameter for many systems [35, 36], including Fe on alumina, as here.

All the CNTs grown on sublimated catalyst wafers result in VA-CNTs with similar macromorphology to their reference counterparts produced with e-beam-Fe (shown in figure 1). However, sub-Fe deposited at 80 °C seems to have a lower areal density. (The 'relative areal density' of figure 2(c), as calculated by the algorithm in figure S2, is 0.62 vs. 0.86 for figure 2(e).). This resulted in less dense, and also wavier, tubes. A similar effect of density on waviness was observed in previous work [37]. From a kinetic point of view, the VA-CNT growth rate (figure 3(a)) is similar in all cases throughout the first 40 μm (120 s) of forest growth. Afterward, growth from sub-Fe-80 is significantly slower than the reference growth, but sub-Fe-100 exhibits the same growth rate of VA-CNTs as the reference, indicating a good possible substitute deposition route that can be performed under milder conditions, and at larger scales on more substrate geometries. The quality of the VA-CNTs (figure 3(b)) also seems comparable, as the I_G/I_D of the reference or sub-Fe-100 (and, to a lesser degree, sub-Fe-80) is practically the same, indicating an equivalent amount of defects. TEM inspection of the tubes grown with the different catalyst precursors shows for all crystalline multiwall morphology a very

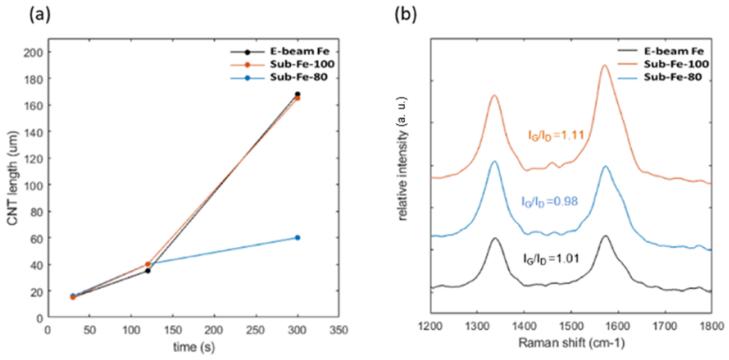


Figure 3. CNT growth rate (a) and Raman spectrum (after 30 s growth) (b) of the CNTs grown on e-beam-Fe, sub-Fe-80, and sub-Fe-100. The CNTs were grown at 740 °C for 300 s for the different catalyst precursors.

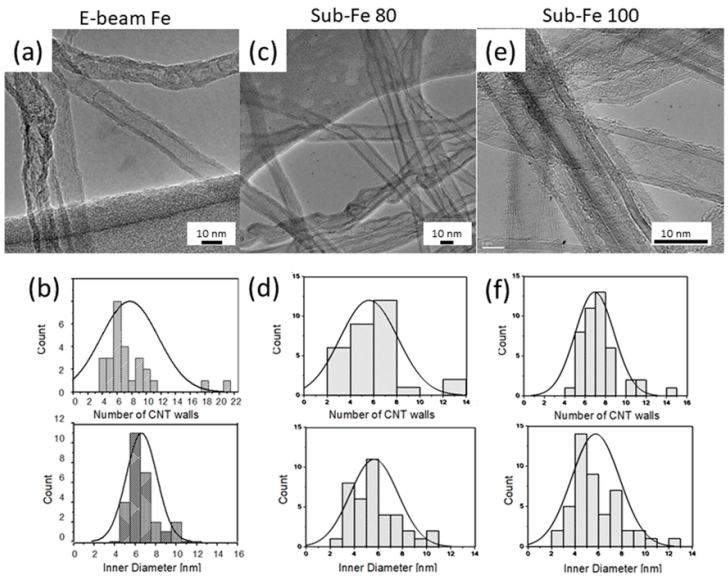


Figure 4. TEM images and respective histograms of the number of walls and inner diameters for CNTs grown with e-beam-Fe (a), (b), sub-Fe-80 (c), (d), and sub-Fe-100 (e), (f). The average inner diameter, outer diameter, and the number of walls for sub-Fe-80 were 5.6 ± 1.9 nm, 8.1 ± 1.7 nm, and 5.6 ± 2.5 nm, respectively, while forsub-Fe-100, they were 5.7 ± 2.0, 10.9 ± 3.6, and 6.9 ± 1.9, respectively.

similar morphology to the e-beam-Fe-grown tubes. Statistical analysis of measurements taken on multiple tubes reports an outer diameter of ∼8 nm with three to eight walls on average (figure 4). This resemblance is expected as, by the time the carbon source is introduced, the temperature of the system is well above the decomposition temperature of ferric chloride (315 °C) and the effective morphology of the Fe catalyst is now identical to e-beam-deposited Fe. High-resolution SEMs of the VA-CNT forests reveal the presence of iron nanoparticles on top of the sub-Fe-grown VA-CNT (figure 2), possibly indicating a tip-growth mechanism for sublimated catalyst precursors. All evidence suggests that sub-Fe-100 is comparable and can be considered an equivalent substitute to Fe e-beam deposition as a catalyst for VA-CNT growth.

Contrarily, VA-CNTs grown by an e-beam-deposited catalyst show no evidence of a residual catalyst as e-beam-Fe is known to generate a base growth. For base vs. tip growth, we performed nanoindentation on sub-Fe-100 to characterize the hardness and reveal different failure modes of the catalyst film as compared to e-beam-Fe. Hardness results shown in figure 5 demonstrate a harder film when deposited by evaporation (0.9 ± 0.47 GPa vs. 0.3 ± 0.09 GPa, respectively). We should also note the evidence of an accentuated plastic deformation in sublimated $FeCl_3$ as opposed to the bottom–up growth.

Further support for base growth induced by e-beam evaporated Fe versus tip growth induced by sub-Fe can be given by the XPS results (figure 6 and table 1). XPS analysis as a function of forest height (top and bottom) of VA-CNTs from e-beam-Fe and sub-Fe-100 shows that the Fe catalyst is concentrated at the bottom of the VA-CNTs grown in the former (i.e. base growth as expected), while it is mostly concentrated on the top for sub-Fe-grown VA-CNTs (i.e. a tip-growth mechanism). Furthermore, a direct correlation

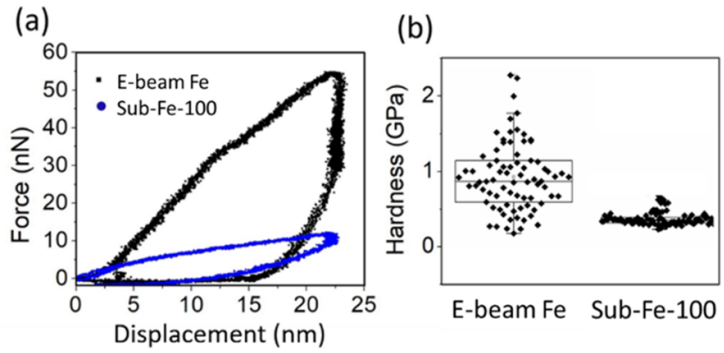


Figure 5. Nanoindentation tests performed on e-beam-Fe and sub-Fe-100 before CNT growth. Representative load vs. displacement curves (a) and calculated hardness (b) for e-beam-Fe and sub-Fe-100 for 50 measurements at different locations on the 2 × 2 cm substrate.

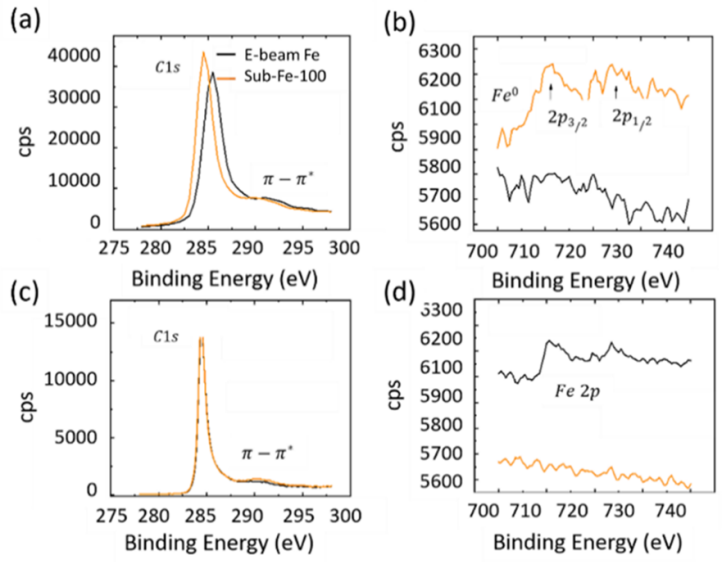


Figure 6. XPS spectra of C (1s) and Fe (2p) binding energy band collected on the top (a), (b) and bottom (c), (d) of a CNT forest grown with e-beam-Fe and sub-Fe-100.

Table 1. XPS surface atomic concentration (%) of bottom and top of VA-CNTs obtained for the control and sublimated catalyst precursor samples.

	Top		Bottom	
	e-beam-Fe	Sub-Fe-100	e-beam-Fe	Sub-Fe-100
C 1s	98.98	98.2	97.31	98.63
O 1s	1.02	1.47	2.58	1.37
Fe 2p	0.0	0.24	0.11	0.0

between the oxygen percentage seen in the elemental XPS analysis and the catalyst location indicates a connection between the catalyst proximity and the oxidative defects concentration. This connection is further supported by the inverse correlation between the height of the $\pi - \pi^*$ peak—indicating undisturbed conjugation between the carbon atoms—and the catalyst location. This correlation between catalyst location and defect concentration can be utilized to tune VA-CNT defects, and thus enable punctuated tailoring of their length-related properties (e.g. negative–positive dipole) for various nanoscale devices.

The electrical properties of VA-CNTs are also explored for the two different growths, as can be seen from comparing sheet resistance and conductivity of knocked-down CNTs, reported in table 2. While e-beam-Fe VA-CNTs show a sheet resistance of ∼50 Ω sq^{-1} and a conductivity of ∼200 S cm^{-1} (slightly better, but in a similar magnitude to previous work [4], which measured sheet resistance of ∼75 Ω sq^{-1} and conductivity of ∼10 S cm^{-1}), VA-CNTs grown from sub-Fe-100 are over 100% more conductive (sheet resistance of

Table 2. Sheet resistance and conductivity of knocked down 100 μms CNT forest.

	e-beam-Fe	Sub-Fe-100
Sheet resistance Ω sq	49.5 ± 3.2	19.9 ± 3.4
Conductivity S cm^{-1}	204 ± 31	530 ± 29.1

~20 Ω sq^{-1} and conductivity of ~530 S cm^{-1}, for CNTs at the same length). The increased conductivity is most likely to be related to the different morphologies created by the different catalyst precursors, shown in previous work [38] to be the key influence in such HA-CNTs achieved via knocking down VA-CNTs. It should be noted that both CNT growth processes create CNTs that are evaluated as having the same nanoscale structure (as is evident by the Raman spectra), and, being multiwalled, they are less susceptible to changes in alignment or the density is less likely to be affected by the catalyst size and distribution [39]. However, another major factor in the enhanced electrical conductivity of sub-Fe-100 could be the presence of the tip-growth metallic catalyst within the measured forest, which would require further study.

4. Conclusions

In this work, we have demonstrated a fast and simple way to deposit catalysts for VA-CNT growth in a method known to be versatile over a large range of topographies. The new catalyst precursor, $FeCl_3$, produces VA-CNTs similar in macro- and nanomorphology to the commonly used e-beam evaporated Fe metal, but different in growth mechanism—tip growth vs. base growth, respectively. This difference is most likely the cause of the difference in oxidative defect concentration and, more importantly, in the mesoscale morphology. Although mostly similar in growth rate and quality, the VA-CNTs via $FeCl_3$ sublimation are noted to have more than twice the electrical conductivity of the reference e-beam-Fe growth. The ease and compatibility with nonflat geometries make the Fe-sublimation process very attractive for yielding VA-CNTs for many applications, including CNT-based sensors and energy storage devices. The next steps for this work include *in-situ* TEM studies on the film transformation to nanoparticles in the C-rich and reducing environment of growth, to confirm the proposed growth mechanism, as well as patterning studies, where it is expected that hard-mask patterning should be possible, as well as studying nonflat-growth substrates.

Data availability statement

All data that support the findings of this study are included within the article (and any supplementary files).

Acknowledgments

This work was supported by Airbus, Boeing, Embraer, Lockheed Martin, Saab A B, Hexcel, TohoTenax (Teijin Carbon America), and ANSYS through MIT's Nano-Engineered Composite aerospace STructures (NECST) Consortium. The authors thank John Kane (MIT) and the entire necstlab at MIT for technical support and advice. This work made use of the Center for Nanoscale Systems at Harvard University, a member of the National Nanotechnology Infrastructure Network, supported (in part) by the National Science Foundation under NSF award number ECS-0335765, utilized the core facilities at the Institute for Soldier Nanotechnologies at MIT, supported in part by the US Army Research Office under contracts W911NF-07-D-0004 and W911NF-13-D-0001, and was carried out in part through the use of MIT's Microsystems Technology Laboratories.

ORCID iDs

Noa Lachman https://orcid.org/0000-0001-7870-6845
Brian L Wardle https://orcid.org/0000-0003-3530-5819

References

[1] Rana M and Asyraf M R M 2016 *Microelectron. Eng.* **162** 93–5
[2] Zhang H, Wang B and Brown B 2020 *Appl. Surf. Sci.* **521** 146349
[3] Castellano R J, Praino R F, Meshot E R, Chen C, Fornasiero F and Shan J W 2020 *Carbon* **157** 208–16
[4] Lee J, Stein I Y, Devoe M E, Lewis D J, Lachman N, Kessler S S, Buschhorn S T and Wardle B L 2015 *Appl. Phys. Lett.* **106** 053110
[5] Sharma P, Pavelyev V, Kumar S, Mishra P, Islam S S and Tripathi N 2020 *J. Mater. Sci., Mater. Electron.* **31** 4399–443
[6] Huang S, Du X, Ma M and Xiong L 2021 *Nanotechnol. Rev.* **10** 1592–623

[7] Bedewy M, Meshot E R, Reinker M J and Hart A J 2011 *ACS Nano* **5** 8974–89
[8] Murakami Y, Chiashi S, Miyauchi Y, Hu M, Ogura M, Okubo T and Maruyama S 2004 *Chem. Phys. Lett.* **385** 298–303
[9] Ramirez A, Royo C, Latorre N, Mallada R, Tiggelaar R M and Monzon A 2014 *Mater. Res. Express* **1** 045604
[10] Esconjauregui S, Whelan C M and Maex K 2009 *Carbon* **47** 659–69
[11] Kumar M and Ando Y 2010 *J. Nanosci. Nanotechnol.* **10** 3739–58
[12] Rydel-Ciszek K, Pacześniak C, Zaborniak I, Błoniarz P, Surmacz K, Sobkowiak A and Chmielarz P 2020 *Processes* **8** 1683
[13] Vanhaecke E, Huang F, Yu Y, Ronning M, Holmen A and Chen D 2011 *Top. Catal.* **54** 986
[14] Wang Y, Luo Z, Li B and Ho P S 2007 *J. Appl. Phys.* **101** 124310
[15] de Los Arcos T, Vonau F, Garnier M G, Thommen V, Boyen H-G and Oelhafen P 2002 *Appl. Phys. Lett.* **80** 2383
[16] Dijon J *et al* 2010 *Carbon* **48** 3953–63
[17] Moisala A, Nasibulin A G, Brown D P, Jiang H, Khriachtchev L and Kauppinen E I 2006 *Chem. Eng. Sci.* **61** 4393–402
[18] Ghaemi F, Ali M, Yunus R and Othman R N 2019 *Synthesis, Technology and Applications of Carbon Nanomaterials* (Amsterdam: Elsevier) p 27
[19] Anisimov A S, Nasibulin A G, Jiang H, Launois P, Cambedouzou J, Shandakov S D and Kauppinen E I 2010 *Carbon* **48** 380–8
[20] Liu D, Luo Q, Wang H and Chen J 2009 *Mater. Des.* **30** 649–52
[21] Zhou W, Rutherglen C and Burke P J 2008 *Nano Res.* **1** 158–65
[22] Yamamoto N, Hart A J, Garcia E J, Wicks S S, Duong H M, Slocum A H and Wardle B L 2009 *Carbon* **47** 551–60
[23] Reina A, Hofmann M, Zhu D and Kong J 2007 *J. Phys. Chem.* C **111** 7292–7
[24] Gao Z, Zhang X, Zhang K and Yuen M M F 2015 *J. Phys. Chem.* C **119** 15636–42
[25] Inoue Y, Kakihata K, Hirono Y, Horie T, Ishida A and Mimura H 2008 *Appl. Phys. Lett.* **92** 213113
[26] Ghemes C, Ghemes A, Okada M, Mimura H, Nakano T and Inoue Y 2013 *Jpn. J. Appl. Phys.* **52** 035202
[27] Blairs S 2006 *J. Chem. Thermodyn.* **38** 1484–8
[28] Bach R D, Shobe D S, Schlegel H B and Nagel C J 1996 *J. Phys. Chem.* **100** 8770–6
[29] Hou H, Schaper A K, Jun Z, Weller F and Greiner A 2003 *Chem. Mater.* **15** 580–5
[30] Barr M C, Rowehl J A, Lunt R R, Xu J, Wang A, Boyce C M, Im S G, Bulović V and Gleason K K 2011 *Adv. Mater.* **23** 3500–5
[31] Song I K, Yu W J, Cho Y S, Choi G S and Kim D 2004 *Nanotechnology* **15** S590
[32] Goktas H, Wang X, Ugur A and Gleason K K 2015 *Macromol. Rapid Commun.* **36** 1283–9
[33] Garcia E J, Wardle B L and Hart A J 2008 *Composites* A **39** 1065–70
[34] Lachman N, Sui X, Bendikov T, Cohen H and Wagner H D 2012 *Carbon* **50** 1734–9
[35] Shukrullah S, Mohamed N M, Shaharun M S and Naz M Y 2016 *Mater. Chem. Phys.* **176** 32–43
[36] Cohen S R and Kalfon Cohen E 2013 *Beilstein J. Nanotechnol.* **4** 815–33
[37] Natarajan B, Lachman N, Lam T, Jacobs D, Long C, Zhao M, Wardle B L, Sharma R and Liddle J A 2015 *ACS Nano* **9** 6050–8
[38] Natarajan B, Stein I Y, Lachman N, Yamamoto N, Jacobs D S, Sharma R, Liddle J A and Wardle B L 2019 *Nanoscale* **11** 16327–35
[39] Chen G, Davis R C, Futaba D N, Sakurai S, Kobashi K, Yumura M and Hata K 2016 *Nanoscale* **8** 162–71
[40] Gharahcheshmeh M H, Robinson M T, Gleason E F and Gleason K K 2021 *Adv. Funct. Mater.* **31** 2008712
[41] Li R *et al* 2019 *Angew. Chem., Int. Ed. Engl.* **58** 1–7